Journal of Physics: Conference Series

PAPER • OPEN ACCESS

A generalized wind turbine cross section as a reduced-order model to gain insights in blade aeroelastic challenges

To cite this article: E. Branlard *et al* 2024 *J. Phys.: Conf. Ser.* **2767** 022005

View the article online for updates and enhancements.

You may also like

- Bat-inspired integrally actuated membrane wings with leading-edge sensing
Stefano Buoso, Benjamin T Dickinson and Rafael Palacios
- Aeroelasticity of compliant span morphing wings
Rafic M Ajaj and Michael I Friswell
- Research on sparse identification method for aeroelastic dynamic response prediction
Jiaming Yu, Hui Qi, Xiangyu Li et al.

This content was downloaded from IP address 192.174.37.51 on 02/07/2024 at 03:04

Journal of Physics: Conference Series **2767** (2024) 022005 doi:10.1088/1742-6596/2767/2/022005

A generalized wind turbine cross section as a reduced-order model to gain insights in blade aeroelastic challenges

E. Branlard[1], J. Jonkman[2], J. H. Porter[3], G. Vijayakumar[2], B. Jonkman[4], M. Singh[4], E. Mayda[4], K.Dixon[4]

[1]University of Massachusetts Amherst, Amherst, MA, USA
[2]National Renewable Energy Laboratory, Golden, CO, USA
[3]Rice University, Houston, TX, USA
[4]Envision Energy, Boulder, CO, USA

E-mail: ebranlard@umass.edu

Abstract. In this work, we present an approach to study the aeroelastic stability of a wind turbine by focusing on the dynamics of a blade cross section. We present a methodology to obtain a reduced-order model of the blade dynamics in the form of generalized cross-sectional quantities that approximates the aerodynamic and structural properties of the full blade. The motivation for the work is to gain a physical understanding of the influence of aerodynamic models such as dynamic wake and dynamic stall on the frequency and damping of the structure using a reduced-order model with low computational cost. The model may be coupled to two-dimensional computational fluid dynamics softwares or engineering unsteady airfoil aerodynamics models accounting for dynamic wake and dynamic stall. In the latter case, we can obtain monolithic state-space forms of the aeroelastic system of equations, which simplifies the determination of the modal parameters and therefore the study of stability. The work investigates wind turbines in operation or at standstill, where vortex-induced vibrations and stall-induced vibrations, respectively, might be an issue. The implementation is made available as part of the open-source Python package WELIB and as part of the open-source unsteady aerodynamic driver of OpenFAST.

1. Introduction

Wind turbine aeroelastic stability is a growing concern as structures become larger and more flexible [1, 2]. Wind turbine aeroelastic solvers provide features to study aeroelastic stability [3, 4]. Still, given the multiple degrees of freedom at play, understanding the key phenomena involved is often challenging. Furthermore, the computational requirements for stability can be significant, limiting the use of stability metrics in the design process. Finally, fully coupled aeroelastic simulations with blade-resolved computational fluid dynamics (CFD) are computationally expensive, and coupled aeroelastic effects (e.g., flutter, stall, and vortex-induced vibration) are active research topics [5, 6, 7, 8]. Therefore, the field can benefit from computationally efficient but representative models to study aeroelastic stability.

In this work, we devise and present a simplified method to analyze the aeroelastic stability of rotors by constructing and studying a "generalized" cross section that is representative of the full blade. The goal is to provide physical insights in the field of rotor aeroelastic stability, including

Content from this work may be used under the terms of the Creative Commons Attribution 4.0 licence. Any further distribution of this work must maintain attribution to the author(s) and the title of the work, journal citation and DOI.
Published under licence by IOP Publishing Ltd

vortex-induced vibration and stall-induced vibration, while keeping the problem computationally efficient and preserving only the first-order effects. The method can be used with engineering models, such as those used in blade element momentum codes, or with two-dimensional (2D) CFD.

The dynamics of a rigid airfoil section under aerodynamic forces is a classic aeroelastic problem [9]. However, in the classic problem 1) the effects of unsteady airfoil aerodynamics and induced velocities are neglected; 2) the dynamics of the section are simplified by neglecting effects related to offsets of the center of mass, elastic center, shear center, and principal axes; and 3) it is not straightforward to relate results from the 2D section to the three-dimensional (3D) problem. Previous studies for wind turbine cross sections are found, e.g., in [10, 11, 12].

In this work, we address the challenges of the three points above. In section 2, we introduce our methodology to reduce the blade dynamics and blade loads into a generalized 2D cross section modeled with three degrees of freedom and a generalized aerodynamic load. In section 3, we discuss the determination of the aerodynamic loads of the 2D cross section and the possibility of writing the aeroelastic equations as a monolithic state-space model. The method can be used with CFD or engineering models. For the latter, we present the equations to include the effects of unsteady airfoil aerodynamics and dynamic wake effects. We implement the equations in two dedicated aeroelastic solvers: a Python-based monolithic solver, and a Fortran-based modular driver as part of OpenFAST.

2. Method of the generalized cross section

2.1. Notations for the 2D section

We consider a 2D blade cross section, identified with the radial coordinate $r = r_{\text{sec}}$ along a blade of radius R. The section is moving in a 2D plane, with coordinates (x, y, θ), where the unit vector $\hat{\boldsymbol{x}}$ is assumed to be normal to the rotor plane. The coordinates represent flapwise, edgewise, and torsional motions of the cross section. The main notations are illustrated in Figure 1 and described in the caption.

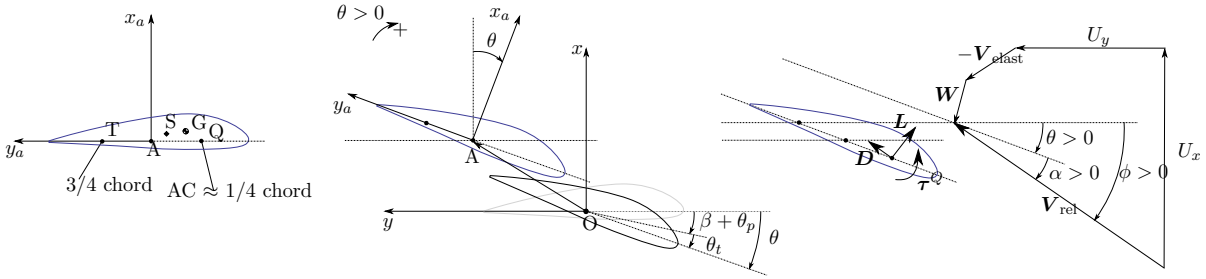

Figure 1. Notations for the aerodynamic models: airfoil origin (A), aerodynamic center (AC, Q), 3/4 chord point (T), center of mass (G), shear center (S), 2D coordinates (x, y, θ_t), relative velocity ($\boldsymbol{V}_{\text{rel}}$), induced velocity ($\boldsymbol{W}$), flow velocity ($\boldsymbol{U}$), aerodynamic lift, drag, and moment ($\boldsymbol{L}$, $\boldsymbol{D}$, $\boldsymbol{\tau}^Q$), reference/blade-root coordinate system ($\hat{\boldsymbol{x}}, \hat{\boldsymbol{y}}, \hat{\boldsymbol{z}}$), airfoil coordinate system ($\hat{\boldsymbol{x}}_a, \hat{\boldsymbol{y}}_a, \hat{\boldsymbol{z}}_a$).

The total angle of the airfoil chord line measured from the y-axis is noted $\theta = \theta_p + \beta + \theta_t$, where θ_p is the pitch angle of the blade, β is the twist angle, and θ_t is the torsional angle resulting from the elastic motion of the blade. We follow the wind energy convention and adopt a negative convention for the angles about the z-axis. Therefore, all the angles presented in Figure 1 are positive.

2.2. Generalized coordinates

To obtain generalized properties that are representative of the full blade, we use a shape function approach [13, 14]. We construct three shape functions (or vector fields), $\underline{\underline{\boldsymbol{S}}} =$

$\{\boldsymbol{S}_f(r), \boldsymbol{S}_e(r), \boldsymbol{S}_t(r)\}$, where r is the radial position along the blade span, bold symbols are vectors and rank 2 tensors (when underlined). For numerical implementation, the vectors are assumed to be column vectors and the tensor coordinates are represented as matrices. The shape functions are illustrated in Figure 2. The shape functions respectively correspond to

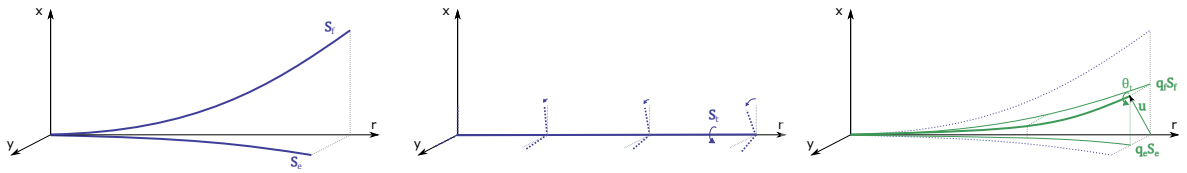

Figure 2. Left: flapwise ($\boldsymbol{S}_f$) and edgewise ($\boldsymbol{S}_e$) shape functions. Middle: Torsional shape function ($\boldsymbol{S}_t$). Right: Motion obtained from the generalized coordinates and shape functions (using $q_f = q_e = 0.5$). In the figure, the shape functions are shown as being purely in their assigned direction; however, a small offset may exist in practice.

displacements of the blade in the flapwise, edgewise, and torsional directions. In this work, they are obtained as a linear combination of three structural and undamped mode shapes of the blade, and we design them such that they are as close as possible to be purely in each of their assigned directions (see subsection 2.5). We introduce three generalized degrees of freedom $\boldsymbol{q} = \{q_f, q_e, q_t\}^T$ that are used to scale the shape functions. At a given time, t, the reference axis of the blade[1] is displaced by the displacement field $\boldsymbol{u}(r)$ [2] as

$$\boldsymbol{u}(r,t) = \{u_x, u_y, \theta_t\}^T = \underline{\boldsymbol{S}}(r)\boldsymbol{q}(t) = q_f(t)\boldsymbol{S}_f(r) + q_e(t)\boldsymbol{S}_e(r) + q_t(t)\boldsymbol{S}_t(r) \tag{1}$$

We include the torsional angle, θ_t, as part of the displacement field for convenience (see footnote 2). An example of displacement field is provided in the right of Figure 2. We chose to scale the shape functions to be unity at the section of interest:

$$\boldsymbol{S}_f(r_{\text{sec}}) = \{1,0,0\}^T, \quad \boldsymbol{S}_e(r_{\text{sec}}) = \{0,1,0\}^T, \quad \boldsymbol{S}_t(r_{\text{sec}}) = \{0,0,1\}^T, \quad \text{i.e.,} \quad \underline{\boldsymbol{S}}(r_{\text{sec}}) = \underline{\mathbb{1}} \tag{2}$$

The scaling, though unnecessary, conveniently ensures that the generalized coordinates ($\boldsymbol{q}(t)$) correspond to the displacements of the section of interest:

$$\boldsymbol{u}(r_{\text{sec}}, t) = \{q_f(t), q_e(t), q_t(t)\}^T = \boldsymbol{q}(t) \tag{3}$$

From the discussion of footnote 1, we assume that the translation displacement can be replaced by the position (i.e., $q_f = x$, $q_e = y$) and $q_t = \theta_t$.

2.3. Generalized aerodynamic loads

An advantage of our approach is that we only use the 2D aerodynamic loads of the cross section of interest. This greatly saves computational time when CFD is used and offers physical

[1] We recall that shape functions represent displacement fields from a reference position. In this work, we assume that the reference position is the blade's position in quasi-static equilibrium under a given operating condition. If the equilibrium is periodic, we may average it to obtain a steady condition. However, we adopt the common approach of eliminating effects that introduce periodicity when performing stability analyses (e.g., removing gravity and ensuring that the inflow is uniform in the direction perpendicular to the rotor). In other words, the equilibrium is computed for an isotropic rotor operating in isotropic external conditions. The reference axis does not need to be straight and may contain prebend, presweep, and twist resulting from the blade's manufacturing and/or quasi-static elastic displacement at a given operating condition. The offsets and rotations will affect how the structural matrices are obtained, influencing factors such as geometrical stiffening. These effects can be included in the shape function formalism (see, e.g., [15]). The prebend and presweep offsets are irrelevant for the description of the 2D cross section (the aerodynamics remain the same if the section is translated). Only the quasi-steady torsion needs to be included, for instance, in β.

[2] In line with footnote 1, for simplicity, we consider that the torsional degree of freedom imparts rotations solely about the main z-axis of the blade, independent of any potential prebend and presweep of the blade. In the general case, the torsional shape function should be represented as a 3×3 transformation field and a displacement field; refer to, for example, [13].

insight. Yet for the method to be successful and indeed represent a "generalized" cross section characteristic of the full blade, we need to relate the 2D loads to the full blade loads. To achieve this, we use a concept similar to the one used for the generalized coordinates: we separate space and time dependencies. We write $\boldsymbol{f}_{\text{sec}}(t) = \{f_x(t), f_y(t), \tau(t)\}$, which are the 2D unsteady aerodynamic loads per unit span, computed based on the 2D airfoil aerodynamics of the cross section, where f_x and f_y are the loads in the x and y directions, and τ is the moment about the z-axis. We assume that the aerodynamic loads per unit span at any cross section along the blade can be obtained based on precomputed aerodynamic shape functions $\underline{\underline{\boldsymbol{S}}}_a(r)$ as

$$\boldsymbol{f}(r,t) = \underline{\underline{\boldsymbol{S}}}_a(r)\boldsymbol{f}_{\text{sec}}(t) = f_x(t)\boldsymbol{S}_{a,x}(r) + f_y(t)\boldsymbol{S}_{a,y}(r) + \tau(t)\boldsymbol{S}_{a,\theta}(r) \tag{4}$$

The aerodynamic shape function can be obtained from an aeroelastic code by extracting the steady-state aerodynamic loads at a given operating condition (identified by wind speed, rotational speed, and pitch angle) and at the steady-state elastic deformation of the blade (see footnote [2]). We note $\{p_x(r), p_y(r), m_z(r)\}$ as the loads extracted from the aeroelastic code at a given operating condition. In this step, we also store the axial and tangential induced velocities (used in subsection 3.5). We set the load shape functions as purely acting in each of their associated degrees of freedom, and we scale them such that they are unity at the section of interest, namely,

$$\boldsymbol{S}_{a,x}(r) = \left\{\frac{p_x(r)}{p_x(r_{\text{sec}})}, 0, 0\right\}^T,\ \boldsymbol{S}_{a,y}(r) = \left\{0, \frac{p_y(r)}{p_y(r_{\text{sec}})}, 0\right\}^T,\ \boldsymbol{S}_{a,\theta}(r) = \left\{0, 0, \frac{m_z(r)}{m_z(r_{\text{sec}})}\right\}^T \tag{5}$$

We will show in subsection 2.5 (Equation 12) that the generalized aerodynamic loads are obtained as

$$\boldsymbol{Q}_a(t) = \{Q_{a,f}, Q_{a,e}, Q_{a,t}\} = \underline{\underline{\boldsymbol{k}}}_a \boldsymbol{f}_{\text{sec}}(t), \quad \text{with} \quad \underline{\underline{\boldsymbol{k}}}_a = \int_0^R \underline{\underline{\boldsymbol{S}}}(r)^T \underline{\underline{\boldsymbol{S}}}_a(r)\,\mathrm{d}r \tag{6}$$

where $\underline{\underline{\boldsymbol{k}}}_a$ are scaling factors obtained by integration of the aerodynamic shape functions against the generalized shape functions.

2.4. Equations of motion from different underlying representations

In structural dynamics of continuous systems, the equations of motion can be obtained in different ways, depending on the representation used (see [16]): collocation, finite element method (FEM), Rayleigh-Ritz, etc. Similarly, the method introduced in subsection 2.2 can be implemented in different ways. In this work, we present two approaches: the Rayleigh-Ritz approach (also called assumed shape function approach) and the finite-element approach. The Rayleigh-Ritz approach employs assumed shape functions and global integrals over the entire span of a body. The FEM approach also relies on shape functions (defined for each nodal degree of freedom), but the end results of the method are vectors and matrices that inherently contain the integrals (or collocation weights) over the body span.

For either approach, the general procedure to obtain the equations of motion of the generalized cross section is as follows:

(i) For a given operating condition, determine the mode shapes of the blade and extract the first flap, edge, and torsional modes.

(ii) Project the three mode shapes into three canonical shape functions that have a value of 1 in each degree of freedom, to form generalized coordinates.

(iii) Integrate the material properties of the blade using these generalized coordinates to obtain generalized mass, damping, and stiffness matrices: $\underline{\underline{\boldsymbol{M}}}$, $\underline{\underline{\boldsymbol{C}}}$, and $\underline{\underline{\boldsymbol{K}}}$, respectively. Each matrix is of shape 3×3, because three generalized degrees of freedom are used. If the damping matrix is not known, modal damping can be used.

(iv) Precompute the generalized force scaling factors, $\underline{\underline{\boldsymbol{k}}}_a$, that convert the aerodynamic

loads of the 2D section, $\boldsymbol{f}_{\text{sec}}$, to generalized aerodynamic loads (see aerodynamic loads subsection 2.3).

At the end, we obtain the equations of motion in the following form:

$$\underline{\underline{\boldsymbol{M}}}\ddot{\boldsymbol{q}} + \underline{\underline{\boldsymbol{C}}}\dot{\boldsymbol{q}} + \underline{\underline{\boldsymbol{K}}}\boldsymbol{q} = \underline{\underline{\boldsymbol{k}}}_a \boldsymbol{f}_{\text{sec}}(\boldsymbol{q}, \dot{\boldsymbol{q}}) \tag{7}$$

In Equation 7, we neglect direct inertial and elastic forces that may introduce nonlinearities, but we keep the nonlinearities due to aerodynamics. A model for the nonlinear structural forces could be included in the future as an additional force. Instead, in this work, we linearize the structural dynamics effects (such as centrifugal loading). We perform modal analyses (linearization) of the nonlinear finite element model at different operating points, to obtain different mode shapes, shape functions and system matrices. Our main goal is to understand how nonlinear aerodynamics affect aeroelastic stability, and therefore, we assume that linear structural dynamics (obtained about an operating point) is sufficient to capture the onset of instabilities. The validity of this assumption remains open to discussion. We detail the different steps for the Rayleigh-Ritz and FEM approach in the following sections.

2.5. Rayleigh-Ritz approach

The Rayleigh-Ritz approach is a natural way to implement the methodology presented above because it relies on assumed shape functions.

(i) In this work, we obtain the mode shapes of the blade (i.e., step (i) in subsection 2.4) using a finite element software (see subsection 2.6). We extract the first flap, edge, and torsional modes of the blade, noted: $\underline{\underline{\boldsymbol{\Phi}}} = \{\boldsymbol{\Phi}_f(r), \boldsymbol{\Phi}_e(r), \boldsymbol{\Phi}_t(r)\}$.

(ii) We obtain the three shape functions, $\underline{\underline{\boldsymbol{S}}}$, as a linear combination of the components of $\underline{\underline{\boldsymbol{\Phi}}}$ such that

$$\underline{\underline{\boldsymbol{S}}}(r) = \underline{\underline{\boldsymbol{T}}}\,\underline{\underline{\boldsymbol{\Phi}}}(r) \tag{8}$$

where $\underline{\underline{\boldsymbol{T}}}$ is the coordinate transformation matrix from mode shapes to shape functions. We determine $\underline{\underline{\boldsymbol{T}}}$ using the scaling introduced in Equation 2:

$$\underline{\underline{\mathbb{1}}} = \underline{\underline{\boldsymbol{S}}}(r_{\text{sec}}) = \underline{\underline{\boldsymbol{T}}}\,\underline{\underline{\boldsymbol{\Phi}}}(r_{\text{sec}}), \quad \Rightarrow \quad \underline{\underline{\boldsymbol{T}}} = \underline{\underline{\boldsymbol{\Phi}}}(r_{\text{sec}})^{-1} \tag{9}$$

The shape functions are then entirely determined from the mode shapes. The process is illustrated in Figure 3. We note that the shape function is not fully contained in a plane, but the condition at r_{sec} is enforced.

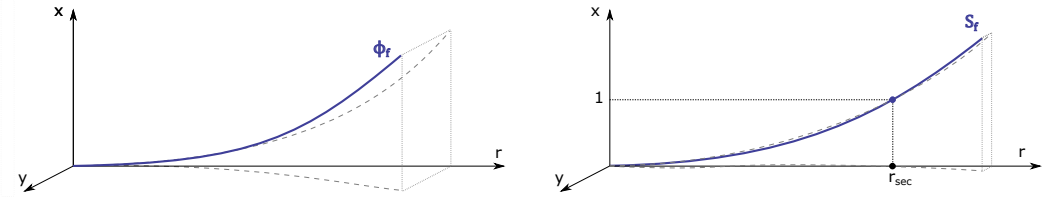

Figure 3. Left: Flapwise mode shape, $\boldsymbol{\Phi}_f$. Right: Flapwise shape function $\boldsymbol{S}_f$ obtained as a combination of the three mode shapes.

(iii) The structural matrices are obtained by integrating the mass and stiffness distribution of the blade against the shape functions. Under the assumptions of this work, the mass matrix is for instance obtained as

$$\underline{\underline{\boldsymbol{M}}} = \int_0^R \underline{\underline{\boldsymbol{S}}}^T \underline{\underline{\boldsymbol{m}}}\,\underline{\underline{\boldsymbol{S}}}\,\mathrm{d}r \tag{10}$$

where $\underline{\underline{\boldsymbol{m}}}$ is the 3×3 matrix of diagonal coefficients $m(r)$, $m(r)$, and $J_{zz}(r)$, where $m(r)$ is the mass per unit length of the beam, and $J_{zz}(r)$ is the mass moment of inertia per unit

length of the beam sections expressed on the beam axis and about the z-axis. The reader is referred to other references for additional details and ways to compute the mass and stiffness matrices, including moment of inertia and geometrical stiffening effects [13, 14, 15].

(iv) In the assumed shape function approach, the generalized loads in each degree of freedom are obtained by integrating the body loads against the shape functions over the whole body:

$$\boldsymbol{Q}(t) = \int_0^R \underline{\underline{\boldsymbol{S}}}^T(r)\boldsymbol{f}(r,t)\,\mathrm{d}r, \qquad \text{e.g.,} \quad Q_e(t) = \int_0^R \boldsymbol{S}_e(r)\cdot\boldsymbol{f}(r,t)\,\mathrm{d}r \tag{11}$$

The generalized aerodynamics loads are then obtained by inserting Equation 4 into Equation 11, leading to

$$\boldsymbol{Q}_a(t) = \left[\int_0^R \underline{\underline{\boldsymbol{S}}}^T(r)\underline{\underline{\boldsymbol{S}}}_a(r)\,\mathrm{d}r\right]\boldsymbol{f}_{\mathrm{sec}} = \underline{\underline{\boldsymbol{k}}}_a\boldsymbol{f}_{\mathrm{sec}}(t) \tag{12}$$

2.6. FEM approach

In the FEM approach, the continuous vector fields are replaced by column vectors defining nodal values. Integrals over the blade span are inherently accounted for by the method. A continuous 3D vector field $\boldsymbol{V}(r)$ is written $\mathbf{V}$ in its FEM form (a discrete vector that stacks the values for the degrees of freedom of each node into a single column vector). The mass and stiffness matrices of the FEM model are noted $\underline{\underline{\mathbf{M}}}_{\mathrm{FE}}$, $\underline{\underline{\mathbf{K}}}_{\mathrm{FE}}$, of shape $n_{\mathrm{FE}} \times n_{\mathrm{FE}}$, where n_{FE} is the number of degrees of freedom of the FEM. These matrices are assumed to be obtained at the quasi-static equilibrium of the blade and contain effects related to geometrical stiffening and boundary conditions. We note $\mathbf{I}_{\mathrm{sec}}$, the indices of the FEM degrees of freedom that correspond to the x, y, and θ displacements. For a given vector $\mathbf{V}$ (or matrix), we write $\mathbf{V}|_{\mathrm{sec}}$, the operation of taking the rows with indices $\mathbf{I}_{\mathrm{sec}}$.

(i) The mode shapes are determined using an eigenvalue value analysis of $\underline{\underline{\mathbf{M}}}_{\mathrm{FE}}$ and $\underline{\underline{\mathbf{K}}}_{\mathrm{FE}}$:

$$\underline{\underline{\mathbf{K}}}_{\mathrm{FE}}\boldsymbol{\Phi} = \lambda\underline{\underline{\mathbf{M}}}_{\mathrm{FE}}\boldsymbol{\Phi} \tag{13}$$

where $\boldsymbol{\Phi}$ is a given mode shape vector and λ is its corresponding eigenvalue. The first flap, edge, and torsional modes are identified based on their deflections and frequencies. They are then concatenated into a $n_{\mathrm{FE}} \times 3$ matrix: $\underline{\underline{\boldsymbol{\Phi}}} = \{\boldsymbol{\Phi}_f, \boldsymbol{\Phi}_e, \boldsymbol{\Phi}_t\}$. We note that the mode shapes are scaled such that

$$\underline{\underline{\boldsymbol{\Phi}}}^T\underline{\underline{\mathbf{M}}}_{\mathrm{FE}}\underline{\underline{\boldsymbol{\Phi}}} = \underline{\underline{\mathbb{1}}}, \qquad \underline{\underline{\boldsymbol{\Phi}}}^T\underline{\underline{\mathbf{K}}}_{\mathrm{FE}}\underline{\underline{\boldsymbol{\Phi}}} = \underline{\underline{\boldsymbol{\Lambda}}} \tag{14}$$

where $\underline{\underline{\boldsymbol{\Lambda}}}$ is the diagonal matrix made of the eigenvalues of the modes.

(ii) We seek a linear transformation of the mode shapes, similar to Equation 9, to obtain the three shape functions, $\underline{\underline{\boldsymbol{S}}}$ (of shape $n_{\mathrm{FE}} \times 3$) such that

$$\underline{\underline{\mathbf{S}}}^T = \underline{\underline{\mathbf{T}}}\,\underline{\underline{\boldsymbol{\Phi}}}^T, \quad \text{given} \quad \underline{\underline{\mathbf{S}}}\big|_{\mathrm{sec}} = \underline{\underline{\mathbb{1}}} \tag{15}$$

We obtain the 3×3 matrix $\underline{\underline{\mathbf{T}}}$ using the amplitudes of the modes at the section

$$\underline{\underline{\mathbf{T}}} = \left[\underline{\underline{\boldsymbol{\Phi}}}\big|_{\mathrm{sec}}\right]^{-1} \tag{16}$$

(iii) We can then compute the generalized mass and stiffness matrices as

$$\underline{\underline{\mathbf{M}}} = \underline{\underline{\mathbf{S}}}^T\underline{\underline{\mathbf{M}}}_{\mathrm{FE}}\underline{\underline{\mathbf{S}}}, \qquad \underline{\underline{\mathbf{K}}} = \underline{\underline{\mathbf{S}}}^T\underline{\underline{\mathbf{K}}}_{\mathrm{FE}}\underline{\underline{\mathbf{S}}} \tag{17}$$

We note that by using Equation 14 and Equation 15, we also have $\underline{\underline{\mathbf{M}}} = \underline{\underline{\mathbf{T}\mathbf{T}^T}}$ and $\underline{\underline{\mathbf{K}}} = \underline{\underline{\mathbf{T}\boldsymbol{\Lambda}\mathbf{T}^T}}$.

(iv) The aerodynamic shape functions given in Equation 5 need to be translated into the FEM model. First, they are evaluated at the quadrature nodes of the FEM model (in BeamDyn, the quadrature nodes are different from the nodes of the FEM model itself). Then, the loads distribution is integrated against the FEM shape functions to obtain nodal values.

The transformed aerodynamic shape functions are concatenated into a $n_{\text{FE}} \times 3$ matrix: $\underline{\underline{\mathbf{S}}}_a = \{\mathbf{S}_{a,x}, \mathbf{S}_{a,y}, \mathbf{S}_{a,\theta}\}$. The aerodynamic scaling factors are then obtained as

$$\underline{\underline{\mathbf{k}}}_a = \underline{\underline{\mathbf{S}}}^T \underline{\underline{\mathbf{S}}}_a \tag{18}$$

We note that while the approach may resemble a modal decoupling method, the method and objectives are distinct: the shape functions introduce structural couplings between the degrees of freedom, and additional couplings are introduced via the aerodynamic scaling factors.

3. 2D unsteady aerodynamics of the section

The steps given in subsection 2.4 provide the equations of motion of the generalized cross section (Equation 7). The inputs to the system are the 2D aerodynamic loads $f_{\text{sec}}(t, \boldsymbol{q}, \dot{\boldsymbol{q}})$. Their determination is the topic of this section. Throughout the section, we rely on the notations provided in Figure 1 and its caption.

3.1. Aerodynamic models

We assume that the structural dynamics and motions are expressed at the airfoil reference point A and that the aerodynamic loads are provided at the aerodynamic center (or "quarter chord" point) Q. The coupling with an external CFD code or with engineering models is achieved consistently through the exchange of two key elements: 1) rigid body kinematics of the cross section at point A and 2) integrated aerodynamic loads at the aerodynamic center Q. In this work, we have implemented two couplings with engineering models: a numerical coupling within the OpenFAST framework [3] and an analytical state-space coupling in Python [17]. A CFD coupling is currently being implemented. The kinematics and loads provided in the following sections are applicable to all couplings.

3.2. Kinematics

The rigid-body kinematics at point A are directly obtained from the degrees of freedom $\boldsymbol{q}$. In this section, for conciseness, we write $\boldsymbol{q} = \{x, y, \theta_t\}^T$ in lieu of $\{q_x, q_y, q_\theta\}^T$. The position, velocity, and acceleration of the airfoil section are

$$\boldsymbol{r}_A = x\hat{\boldsymbol{x}} + y\hat{\boldsymbol{y}}, \qquad \dot{\boldsymbol{r}}_A = \dot{x}\hat{\boldsymbol{x}} + \dot{y}\hat{\boldsymbol{y}}, \qquad \ddot{\boldsymbol{r}}_A = \ddot{x}\hat{\boldsymbol{x}} + \ddot{y}\hat{\boldsymbol{y}} \tag{19}$$

The rotational speed and acceleration of the section are: $\boldsymbol{\omega} = -\dot{\theta}_t\hat{\boldsymbol{z}}$ and $\dot{\boldsymbol{\omega}} = -\ddot{\theta}_t\hat{\boldsymbol{z}}$. For a point, P, located at coordinates (x'_{AP}, y'_{AP}) in the airfoil coordinate system (typically the points of interests are Q or T), its position is $\boldsymbol{r}_P = \boldsymbol{r}_A + \boldsymbol{r}_{AP}$, with $r_{AP} = (x'_{AP}\cos\theta + y'_{AP}\sin\theta)\hat{\boldsymbol{x}} + (-x'_{AP}\sin\theta + y'_{AP}\cos\theta)\hat{\boldsymbol{y}}$. Its velocity is $\boldsymbol{V}_{\text{elast}} = \dot{\boldsymbol{r}}_P = \dot{\boldsymbol{r}}_A + \boldsymbol{\omega} \times \boldsymbol{r}_{AP}$. The acceleration is $\ddot{\boldsymbol{r}}_P = \ddot{\boldsymbol{r}}_A + \dot{\boldsymbol{\omega}} \times \boldsymbol{r}_{AP} + \boldsymbol{\omega} \times (\boldsymbol{\omega} \times \boldsymbol{r}_{AP})$.

3.3. Inflow

We write $\boldsymbol{U} = U_x\hat{\boldsymbol{x}} + U_y\hat{\boldsymbol{y}}$ as the inflow velocity at the airfoil section, corresponding to the wind velocity if the section was not present (no induced velocity, no structural velocity). For the study of a wind turbine section, we assume that U_y contains the contribution of the blade rotation ("Ωr")[3]. We write $\boldsymbol{V} = \boldsymbol{U} - \boldsymbol{V}_{\text{elast}} = V_x\hat{\boldsymbol{x}} + V_y\hat{\boldsymbol{y}}$ as the relative wind perceived by the section consisting of the elastic motion and the wind.

For lifting-line models, we define the relative flow velocity, V_{rel}, which includes wind, structural motion, and induced velocities, as

$$\boldsymbol{V}_{\text{rel}} = \boldsymbol{U} - \boldsymbol{V}_{\text{elast}} + \boldsymbol{W} \tag{20}$$

[3] This contribution is usually considered to be part of the elastic velocity in wind turbine aerodynamic codes, but for the study of a section, the contribution from the rotation is considered to be similar to the inflow.

where $\boldsymbol{W}$ is the induced velocity. The angle of attack, α, and flow angle, ϕ, are defined as

$$\alpha = \phi - \theta = \phi - (\theta_t + \theta_p + \beta), \quad \phi = \arctan \frac{V_{\text{rel},x}}{V_{\text{rel},y}} \tag{21}$$

In numerical applications, arctan is computed using a quadrant-based function (typically `atan2`). When applicable, we will use a subscript Q or T to indicate whether a variable is expressed at a given point. For instance, the relative velocity at the 3/4 chord point (T), is obtained using subsection 3.2 as

$$\begin{aligned} \boldsymbol{V}_{\text{rel}}^T = &\left[U_x - \dot{x} - \dot{\theta}(-x'_{AT}\sin\theta + y'_{AT}\cos\theta) + W_x\right]\hat{\boldsymbol{x}} \\ &+ \left[U_y - \dot{y} + \dot{\theta}(x'_{AT}\cos\theta + y'_{AT}\sin\theta) + W_y\right]\hat{\boldsymbol{y}} \end{aligned} \tag{22}$$

We note that when 2D CFD is used, aerodynamic loads are determined by the solver directly and there is no need to determine the angle of attack or relative wind speed.

3.4. Aerodynamic loads

The component of the aerodynamic loads (per unit length) at the aerodynamic center (Q) and in the reference frame are noted F_x, F_y, τ^Q. The torque τ^Q is assumed positive about the z-axis and is transferred to point A as follows:

$$\tau^A = \tau^Q - F_x(-x'_{AQ}\sin\theta + y'_{AQ}\cos\theta) + F_y(x'_{AQ}\cos\theta + y'_{AQ}\sin\theta) \tag{23}$$

where x'_{AQ} and y'_{AQ} is the location of the aerodynamic center in the airfoil coordinate system. If A is at the midchord, typical values are $y'_{AQ} = 0$ and $x'_{AQ} = -0.25c$ where c is the airfoil chord.

For engineering models, the aerodynamic loads are expressed as lift, drag, and moment:

$$L = \frac{1}{2}\rho c V_{\text{rel}}^2 C_{l,\text{dyn}}, \quad D = \frac{1}{2}\rho c V_{\text{rel}}^2 C_{d,\text{dyn}}, \quad \tau^Q = \frac{1}{2}\rho c^2 V_{\text{rel}}^2 C_{m,\text{dyn}} \tag{24}$$

where ρ is the air density, and $C_{l,\text{dyn}}$, $C_{d,\text{dyn}}$, $C_{m,\text{dyn}}$ are the unsteady lift, drag, and moment coefficients, respectively. They are projected in the reference frame and transferred to A as follows:

$$\begin{aligned} F_x &= L\cos\phi + D\sin\phi = \frac{1}{2}\rho c V_{\text{rel}}^2 \left[C_{l,\text{dyn}}\cos\phi + C_{d,\text{dyn}}\sin\phi\right] \\ F_y &= -L\sin\phi + D\cos\phi = \frac{1}{2}\rho c V_{\text{rel}}^2 \left[-C_{l,\text{dyn}}\sin\phi + C_{d,\text{dyn}}\cos\phi\right] \\ \tau^A &= \frac{1}{2}\rho c V_{\text{rel}}^2 \left[cC_{m,\text{dyn}} - C_{l,\text{dyn}}\left(y'_{AQ}\cos\alpha + x'_{AQ}\sin\alpha\right) + C_{d,\text{dyn}}\left(x'_{AQ}\cos\alpha - y'_{AQ}\sin\alpha\right)\right] \end{aligned} \tag{25}$$

In the above equations, it is important to express V_{rel}, ϕ, and α at the same point (typically Q) for the projection to be valid. Internally, models may use variables at other locations.

3.5. Induced velocity - dynamic wake (engineering model only)

We implement a frozen wake (quasi-steady) or dynamic wake approach for the induced velocities. The dynamic wake model accounts for the slow variation of induced velocities when the loads on the rotor change and therefore when the wake state changes. We define the quasi-steady induced velocity using the relative wind at the aerodynamic center:

$$\boldsymbol{W}_{\text{qs}}(t) = -a_{\text{qs}} V_x^Q(t)\hat{\boldsymbol{x}} + a'_{\text{qs}} V_y^Q(t)\hat{\boldsymbol{y}} \tag{26}$$

where a_{qs} and a'_{qs} are the axial and tangential induction factors, respectively, assumed constant for a given operating point and precomputed according to subsection 2.3. We assume that the induction vector is the same at the points Q and T. The quasi-steady induced velocity will vary with time due to changes of relative wind $\boldsymbol{V}$. In the frozen wake approach

$$\boldsymbol{W} = \boldsymbol{W}_{\text{qs}} \tag{27}$$

For the dynamic wake representation, we use Øye's dynamic wake model [18] with the specific implementation given in [19]. The model uses four states: $\boldsymbol{q}_{dw} = \{W_{x,r}, W_{y,r}, W_x, W_y\}^T$ where $W_{x,r}$ and $W_{y,r}$ are intermediate induced velocities.

3.6. Unsteady airfoil aerodynamic model (engineering model only)

The unsteady airfoil aerodynamics model accounts for dynamic stall and shed vorticity effects and provides the unsteady lift, drag, and moment coefficients ($C_{l,\mathrm{dyn}}$, $C_{d,\mathrm{dyn}}$, and $C_{m,\mathrm{dyn}}$). In the Python version of our implementation, two models are available: Oye's dynamic stall model [20, 21] and the HGM model (Hansen et al. incompressible state-space version of the Beddoes-Leishman model) [22, 19]. Oye's model uses one time-continuous state ($\boldsymbol{q}_{\mathrm{ua}} = \{f_s\}$), whereas the HGM model uses four states ($\boldsymbol{q}_{\mathrm{ua}} = \{x_1, x_2, x_3, x_4\}^T$). In the OpenFAST version [3], six models are available, including the two mentioned above.

3.7. Monolithic and modular formulation (engineering model only)

The Python version of our model implements the full aeroelastic system using a monolithic state-space approach. The state vector is set as the concatenation of the structural and aerodynamic states: $\boldsymbol{x} = \{\boldsymbol{q}^T, \dot{\boldsymbol{q}}^T, \boldsymbol{q}_{\mathrm{ua}}^T, \boldsymbol{q}_{\mathrm{dw}}^T, \}^T$. We set the input vector to be $\boldsymbol{u} = \{U_x, U_y, \theta_p\}^T$. The equations of motion (Equation 7) and the engineering aerodynamic models presented in this section are then gathered into a state equation of the form $\dot{\boldsymbol{x}} = \boldsymbol{F}(t, \boldsymbol{x}, \boldsymbol{u})$. The state equation is readily linearized using numerical differentiation to obtain a linearized state-space matrix $\underline{\underline{\boldsymbol{A}}}$. An eigenvalue analysis of $\underline{\underline{\boldsymbol{A}}}$ provides the modal parameters, including the natural frequencies and damping.

The OpenFAST version uses a modular approach [23]. The linearization process is slightly more involved but is based on the same principles.

4. Conclusion

This work introduces a novel methodology to obtain a reduced-order aeroelastic model of a blade. The reduced-order model is built as a generalized 2D cross section with three degrees of freedom, and it only uses the aerodynamic loads of the cross section as input. The simplicity of the model makes it possible to gain physical insights in the field of rotor aeroelastic stability, including vortex-induced vibration and stall-induced vibration. We note though, that these phenomena are inherently three dimensional, and the method developed here is only intended as a first step to understanding these phenomena. The model may be coupled to engineering models, or, thanks to its computational efficiency, 2D CFD. We provide two open-source implementations of the method as part of WELIB v1.1 [17] and OpenFAST v4.0 [3].

Future work will include comparisons with blade-resolved CFD to study the onset of stall-induced vibrations and additional verification of the methods by comparing them to full rotor linearization results.

References

[1] D. M. Volk, B. S. Kallesøe, S. Johnson, G. R. Pirrung, R. Riva, and F. Barnaud, "Large wind turbine edge instability field validation," *Journal of Physics: Conference Series*, vol. 1618, p. 052014, sep 2020.

[2] C. Grinderslev, F. Houtin-Mongrolle, N. Nørmark Sørensen, G. Raimund Pirrung, P. Jacobs, A. Ahmed, and B. Duboc, "Forced-motion simulations of vortex-induced vibrations of wind turbine blades – a study of sensitivities," *Wind Energy Science*, vol. 8, no. 10, pp. 1625–1638, 2023.

[3] B. Jonkman, R. M. Mudafort, A. Platt, E. Branlard, M. Sprague, J. Jonkman, G. Vijayakumar, M. Buhl, H. Ross, P. Bortolotti, M. Masciola, S. Ananthan, M. J. Schmidt, J. Rood, R. Damiani, N. Mendoza, M. Hall, and R. Corniglion, "Openfast v4.0.0. open-source wind turbine simulation tool, available at `http://github.com/OpenFAST/OpenFAST/`," 2024.

[4] M. Hansen, "Aeroelastic stability analysis of wind turbines using an eigenvalue approach," *Wind Energy*, vol. 7, no. 2, pp. 133–143, 2004.

[5] P. Pourazarm, Y. Modarres-Sadeghi, and M. Lackner, "A parametric study of coupled-mode flutter for mw-size wind turbine blades," *Wind Energy*, vol. 19, no. 3, pp. 497–514, 2016.
[6] R. Riva, S. Cacciola, and C. L. Bottasso, "Periodic stability analysis of wind turbines operating in turbulent wind conditions," *Wind Energy Science*, vol. 1, no. 2, pp. 177–203, 2016.
[7] D. T. Griffith and M. Chetan, "Assessment of flutter prediction and trends in the design of large-scale wind turbine rotor blades," *Journal of Physics: Conference Series*, vol. 1037, p. 042008, jun 2018.
[8] C. Grinderslev, F. Houtin-Mongrolle, N. Nørmark Sørensen, G. Raimund Pirrung, P. Jacobs, A. Ahmed, and B. Duboc, "Forced-motion simulations of vortex-induced vibrations of wind turbine blades – a study of sensitivities," *Wind Energy Science*, vol. 8, no. 10, pp. 1625–1638, 2023.
[9] R. Bisplinghoff, H. Ashley, and R. Halfman, *Aeroelasticity*. Dover Books on Aeronautical Engineering Series, Dover Publications, 1996.
[10] M. H. Hansen, "Aeroelastic instability problems for wind turbines," *Wind Energy*, vol. 10, pp. 551–577, 2007.
[11] J. Johansen, "Unsteady Airfoil Flows with Application to Aeroelastic Stability," Tech. Rep. Risø-R-1116(EN), Risø National Laboratory, Roskilde, Denmark, October 1999.
[12] C. L. Kelley and J. Paquette, "Investigation of flutter for large, highly flexible wind turbine blades," *Journal of Physics: Conference Series*, vol. 1618, p. 052078, sep 2020.
[13] O. Wallrapp, "Standardization of flexible body modeling in multibody system codes, part i: Definition of standard input data.," *Journal of Structural Mechanics*, vol. 22, no. 3, pp. 283–304, 1994.
[14] E. Branlard and J. Geisler, "A symbolic framework to obtain mid-fidelity models of flexible multibody systems with application to horizontal-axis wind turbines," *Wind Energy Science*, 2022.
[15] E. Branlard, "Flexible multibody dynamics using joint coordinates and the Rayleigh-Ritz approximation: The general framework behind and beyond Flex," *Wind Energy*, vol. 22, no. 7, pp. 877–893, 2019.
[16] A. Nayfeh and P. Pai, *Linear and Nonlinear Structural Mechanics*. Wiley Series in Nonlinear Science, Wiley, 2008.
[17] E. Branlard, "WELIB v1.1.0, Wind Energy Library, GitHub repository `http://github.com/eBranlard/welib/`, `https://doi.org/10.5281/zenodo.8048349` last accessed january 2024," 2024.
[18] H. Snel and J. G. Schepers, "Joint investigation of dynamic inflow effects and implementation of an engineering method," tech. rep., ECN-C–94-107, Energy Research Centre of the Netherlands, Petten, 1995.
[19] E. Branlard, B. Jonkman, G. R. Pirrung, K. Dixon, and J. Jonkman, "Dynamic inflow and unsteady aerodynamics models for modal and stability analyses in openfast," *Journal of Physics: Conference Series*, pp. 1–12, 2022.
[20] S. Øye, "Dynamic stall, simulated as a time lag of separation," *Proceedings of the 4th IEA Symposium on the Aerodynamics of Wind Turbines, Rome, Italy, 20-21 Nov 1990*, 1991.
[21] E. Branlard, *Wind Turbine Aerodynamics and Vorticity-Based Methods: Fundamentals and Recent Applications*. Springer International Publishing, 2017.
[22] M. Hansen, M. Gaunaa, and H. Aagaard Madsen, "A Beddoes-Leishman type dynamic stall model in state-space and indicial formulations," tech. rep., Risø National Laboratory, Roskilde, Denmark, 2004.
[23] J. Jonkman, "The New Modularization Framework for the FAST Wind Turbine CAE Tool," Tech. Rep. NREL/CP-5000-57228, National Renewable Energy Laboratory, Grapevine, Texas, 2013.

Acknowledgements
This work was authored in part by the National Renewable Energy Laboratory, operated by Alliance for Sustainable Energy, LLC, for the U.S. Department of Energy (DOE) under Contract No. DE-AC36-08GO28308. Funding provided by the U.S. Department of Energy Office of Energy Efficiency and Renewable Energy Wind Energy Technologies Office. The views expressed in the article do not necessarily represent the views of the DOE or the U.S. Government. The U.S. Government retains and the publisher, by accepting the article for publication, acknowledges that the U.S. Government retains a nonexclusive, paid-up, irrevocable, worldwide license to publish or reproduce the published form of this work, or allow others to do so, for U.S. Government purposes.